STM Investigation of $Y[C_6S\text{-}Pc]_2$ Complex at the Solution/Solid Interface: Substrate Effects, Sub-molecular Resolution, and Vacancies

Shammi Rana, Jianzhuang Jiang,† Katalin V. Korpany, Ursula Mazur, and K. W. Hipps*

Department of Chemistry and Materials Science and Engineering Program, Washington State University, Pullman, WA 99163-4630.

† Department of Chemistry, University of Science and Technology Beijing, Beijing, 100083, China.

ABSTRACT

Substituents present on a molecule are known to significantly control the assembly, adsorption, and orientation behavior on solid surfaces. Using scanning tunneling microscopy (STM), self-assembly of the Y[C_6S-Pc]$_2$ and Y[C_4O-Pc]$_2$ double-decker complexes were investigated at a solution-solid interface. At concentrations above 1 μM, Y[C_6S-Pc]$_2$ formed well-defined monolayers with low defect density on highly oriented pyrolytic graphite (HOPG). On Au(111), on the other hand, it formed dense groups of small islands with some isolated molecules. There was a clear preference for multiples of 15 degrees between the orientations of the islands. A clear visualization of the Y[C_6S-Pc]$_2$ inner molecular structure, including all eight of the sulfur atoms linked to the top phthalocyanine ring, was achieved. At concentrations below 1 μM, stable isolated single molecules were observed only on Au(111), not on HOPG. The thiol linked side chains favor strong adsorption on Au(111) surface, with isolated single molecules being easily visualized and stable over several image scans. At concentrations where well-defined monolayers form, we observe defects in the form of molecular vacancies whose number can be controlled by bias voltage. The enhanced stability of the S-linked system over an O-linked system is demonstrated by comparison with Y[C_4O-Pc]$_2$ and discussed in terms of the organic sulfide-gold interaction. On both HOPG and Au(111) isolated molecules of Y[C_4O-Pc]$_2$ are never observed, Even at very low solution concentrations small rafts of molecules on an otherwise open substrate surfaces are observed. On HOPG the structure of the Y[C_4O-Pc]$_2$ monolayer is complex with both an open and filled cubic structure occurring as a mixed structure. The surface structures seen with either double-decker on HOPG and of Y[C_4O-Pc]$_2$ are probably controlled by equilibrium thermodynamics. The structure of the Y[C_6S-Pc]$_2$ complex on Au(111) is determined by the kinetic barrier to diffusion across the gold surface and is therefore kinetically trapped. We suggest that core moieties with peripheral S-linked alkanes may generally be particularly strong adsorbates on gold. Density functional calculations suggest that the S-linked alkane substituent system may be as much as 1 eV more stable on Au than a similar O-linked system. We have also observed that the Y[C_6S-Pc]$_2$ monolayer on HOPG has a bias and setpoint current dependent defects. At constant tunneling current, less negative bias generates a greater number of vacancies as compared to high negative bias. Consecutive STM scanning shows the diffusion, disappearance, and appearance of new vacancies which are induced both thermally and by the STM tip. This work demonstrates the important role of molecule-substrate interactions, bias voltage, tunneling current, and STM tip on controlling and stabilizing molecular assembly.

1. INTRODUCTION

Self-assembly of molecules into well-defined supramolecular architectures is a significant technique in the so-called “bottom-up” method for making electronic devices from single molecules.[1-3] Self-assembly at the solid-liquid or solid-vacuum interface has gained widespread attention because of its fundamental importance and potential applications in surface science and nanotechnology.[1,4,5] To make a premeditated self-assembly with desired surface chemistry and physical properties, molecules with a well-defined chemical structure and distinctive properties

are needed.[1] In addition to the structure of molecules, other aspects, such as concentration,[6,7] nature of substrate, temperature,[8,9] external stimuli, and solvent[10] play essential roles in controlling the molecular assembly on a surface. Also, the delicate equilibrium between molecule-substrate and molecule-molecule interactions always determines the successful formation of a well-ordered molecular assembly. Therefore, understanding of such interactions is important to fabricate surface nanostructures and molecular devices with desirable function. Stronger molecule-substrate interactions can even interrupt the homogeneous growth of the supramolecular structures on a surface.[11] Thus, the substrate plays an important role in guiding the molecular ordering in distinctive directions and their resulting properties.[12,13]

As a model molecule, phthalocyanine (Pc) and its derivatives are extensively studied for self-assembly because of their planar molecular structure, long π-conjugation, biological relevance, and superior electronic properties.[14-16] Sandwich complexes containing two Pc rings held in close proximity by a lanthanide metal ion -- so-called double-decker (DD) complexes -- represent extended conjugated systems, possessing interesting optical, and electronic properties.[17] Also, DD sandwich complexes belongs to the non-planar phthalocyanine complexes.[15] Most importantly, lanthanide-based DD complexes have received great attention due to their single-molecule magnet (SMM) behavior which makes them promising candidates for molecular spintronics and quantum computing.[18,19] Preparation of ordered self-assemblies of DD complexes on suitable surfaces is important in producing functional materials of these chemical species. Introducing appropriate alkyl side chains into a DD complex is an accepted technique improve solubility and to assist in defining the final structure through side chain spacing and interdigitation on the surface.[14] The self-assembly, structure, and electronic properties of DD complexes have been investigated with STM on different substrates such as Co(111),[20] Au(111),[21] H−Si(001),[22] Cu(111),[23] and highly oriented pyrolytic graphite (HOPG).[19, 24] The face-on adsorption of the Pc ring of DD complexes on solid surfaces facilitates the exploration of electronic properties by high-resolution STM.[14] Furthermore, STM allows direct observation of single-molecular rotation in DD complexes which is an essential element for understanding molecular machines.[25-26]

To date, most of the STM studies on DD complexes at the solution-solid interface were implemented on HOPG surface.[27] Weiss and co-workers have observed two-dimensional crystal growth and stacking of DD complexes at the 1-phenyloctane (PO)/HOPG interface.[28] There were numerous reports on submolecular resolution of DD at the vacuum-solid interface at low temperature but a clear visualization of the inner structure of the DD at solution-solid interface was not achieved in previous literature.[27] To the best of our knowledge, there are few reports on the STM of DD complexes at solution-Au(111) interface and the majority of these were done in electrochemical cells.[29]

Herein, self-assembly of homoleptic DD complexes, $Y[C_6S\text{-}Pc]_2$ where C_6S-Pc is 2,3,9,10,16,17,23,24-octakis(hexylthio)phthalocyaninato and $Y[C_4O\text{-}Pc]_2$ where C_4O-Pc is 2,3,9,10,16,17,23,24-octakis(butyloxy)phthalocyaninato, are investigated by STM at the solution-solid interface. The spontaneous adsorption of these complexes at the 1-PO/HOPG or Au(111)

interface was observed at room temperature. Interestingly, STM results reveals that while Y[C_6S-Pc]$_2$ forms long-range ordered monolayers on the HOPG surface. Small, ordered grains with randomly oriented isolated molecules are seen on the Au(111) surface. The effect of concentration on self-assembly at both HOPG and Au(111) surfaces were also studied. We also observed surface defects in the form of holes or molecular vacancies in the Y[C_6S-Pc]$_2$ monolayers on HOPG. The number of these vacancies can be controlled by bias voltage and tunneling current.

2. THEORETICAL AND EXPERIMENTAL METHODS

Materials. Y[C_6S-Pc]$_2$ and Y[C_4O-Pc]$_2$ complexes were synthesized as described below. 1-Phenyloctane (>98.0%) was obtained from TCI America (Portland, OR, USA) and used as solvent without further purification. HOPG substrates used were 1 cm^2 in size and obtained from SPI (grade 2; West Chester, PA, USA). STM tips were prepared by mechanically cutting Pt/Ir wire (80:20 Pt/Ir, 0.011 in. diameter). Epitaxial Au(111) films with well-defined terraces and single atomic steps were prepared on mica by previously described methods.[30,31] These films were 0.1–0.2 μm thick and had a mean single grain diameter of about 0.5 μm. Unlike true single-crystal gold, these small crystal grains showed reconstruction line spacing ranging from 6.3 to about 9.0 nm.

Synthesis of Y[C_6S-Pc]$_2$ and Y[C_4O-Pc]$_2$: Y[C_6S-Pc]$_2$[32] and Y[C_4O-Pc]$_2$ [33] were synthesized according to the published procedures. For the synthesis of Y[C_6S-Pc]$_2$, a mixture of 4,5-bishexylthiophthalonitrile (141 mg, 0.40 mmol), Y(acac)$_3$·2H_2O (22 mg, 0.050 mmol), and DBU (25 μl) in dry n-pentanol (2.0 mL) was heated to reflux under nitrogen for 8 h. After being cooled to room temperature, the volatiles were removed under reduced pressure and the residue was purified by chromatography on a silica-gel column with $CHCl_3$ as the eluent. The crude product was purified by repeated chromatography followed by recrystallization from $CHCl_3$ and methanol, giving the pure target compound Y[C_6S-Pc]$_2$ as a dark green powder in the yield of 39 mg (24%). As for the synthesis of Y[C_4O-Pc]$_2$, by using the preparation procedure of Y[C_6S-Pc]$_2$ with 4,5-dibutoxyphthalonitrile (109 mg, 0.40 mmol) instead of bishexylthiophthalonitrile (141 mg, 0.40 mmol) as the staring material, Y[C_4O-Pc]$_2$ was also obtained as a dark green powder in the yield of 43 mg (33%).

***In situ* STM Measurements.** The experimental layout is shown in Figure 1a. A 10 μm stock solutions of Y[C_6S-Pc]$_2$ and Y[C_4O-Pc]$_2$ complexes were prepared by dissolving these in 1-phenyloctane and stored in the dark at room temperature (RT), until use. To make samples for STM measurements, 10 to 15 μL of 0.3 to 30 μM solution of Y[C_6S-Pc]$_2$ or Y[C_4O-Pc]$_2$ complex in 1-phenyloctane (1-PO) was deposited on freshly cleaved HOPG or Au(111) substrate in a custom-made solution cell fitted with a Kalrez o-ring (McMaster-Carr, Elmhurst IL, USA). All STM measurements were performed in constant-current mode using a Molecular Imaging Pico Plus Scanning Probe Microscope (SPM) equipped with a 1 μm STM scanner. STM images were obtained using bias voltages ranging from +1.00 to -1.00 V and a set-point current of 10 to 250 pA. STM images were analyzed by using SPIP 6.7.8 software.

Computational Methods. Computations were performed with periodic density functional theory (DFT) using Vienna Ab-initio Simulation Package (VASP)[34,35] version 5.4.4. or with the program Gaussian 09.[36] The single molecule DFT calculations on $Y[C_6S\text{-}Pc]_2$ and $Y[HS\text{-}Pc]_2$ were performed using the UB3LYP functional and the 3-21G basis for C, N, H, and S and the lanl2dz basis for Y. All Gaussian calculations were made on single molecules in the gas-phase.

The VASP code uses the projector augmented wave (PAW) method[35,37] to describe the core electrons and valence–core interactions. We used optPBE-vdW functional[38,39] with PAW potentials optimized for the PBE functional[40] for all calculations. The electronic wavefunctions are sampled using a 5×5×1 Gamma centered k-point grid. A plane wave cut off energy of 550 eV was used for all simulations. Methfessel–Paxton smearing was used to set the partial occupancies for each wave function with a smearing width of 0.2 eV. All the geometries were fully optimized up to ~0.001 eV energy and less than 0.02 forces. The choice of our DFT methodology, plane wave cutoff energies and k-point choice was based on previous periodic DFT simulations of similar systems of type[41-46] and size.[47] Additional computational details are presented in the Electronic Supplementary Information, ESI. VASP calculations for species on Au were performed i) on a supercell composed of three layers of 3×3 Au(111) with the bottom two layers frozen at the experimental crystal structure, ii) upon a supercell having a single molecule adsorbed in an initially flat structure on the above Au, and upon a single adsorbate (without Au) all in the same size supercell. Adsorbate density was less than 1 monolayer. Calculations on graphite were performed on similar sized supercells but with only 2 layers of graphite and the bottom layer fixed at the experimental geometry

3. RESULTS AND DISCUSSION

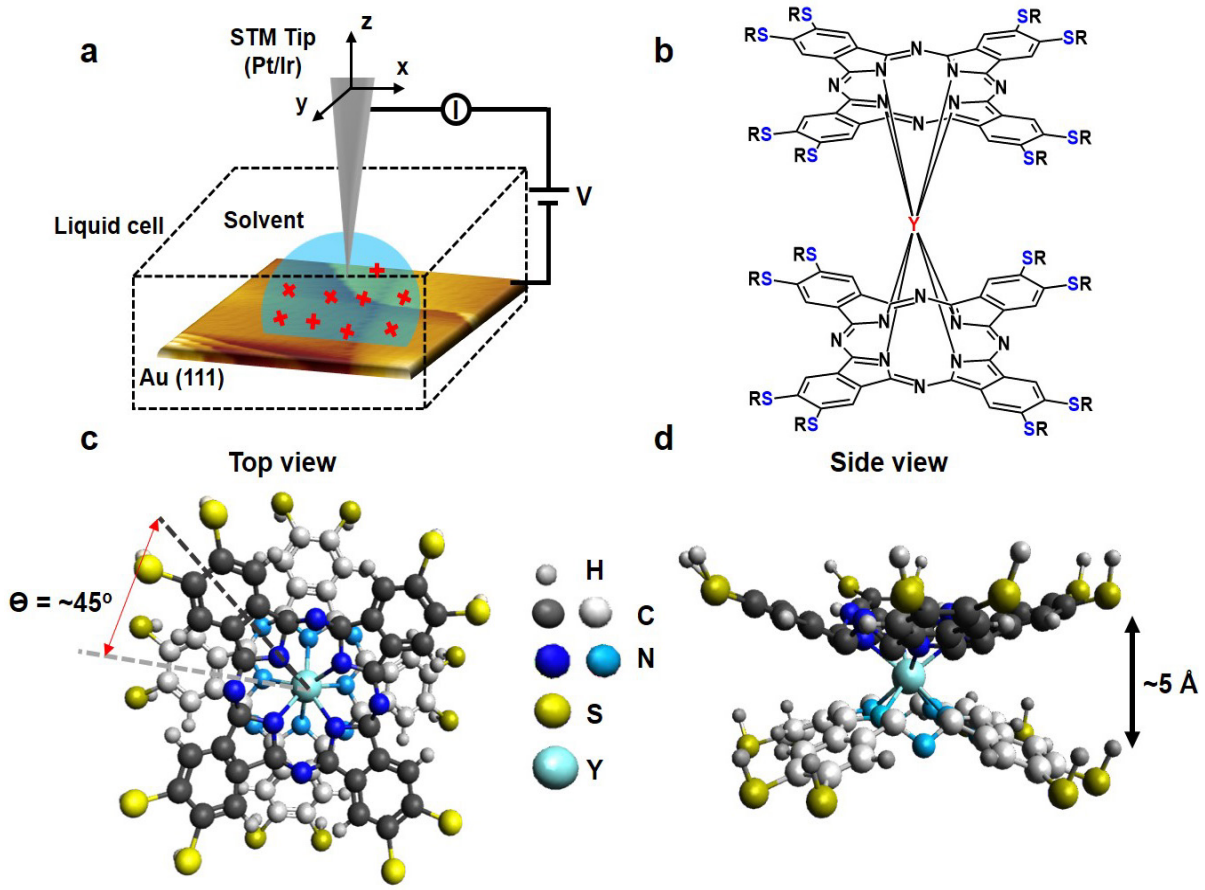

Figure 1: a) Diagrammatic representation of the in situ STM set-up at room temperature, with a representative $Y[C_6S\text{-}Pc]_2$ molecules adsorbed on Au(111) at the solution-solid interface. b) Molecular structure of $Y[RS\text{-}Pc]_2$ complex, where R = $-C_6H_{13}$. Top view (c) and side view (d) of $Y[RS\text{-}Pc]_2$ molecules, here R is replaced with hydrogen for simplicity. Bottom Pc ring is shown in lighter colors for clarity. Top view represents 45° angle between top and bottom Pc ligand while side view shows doom shaped structure of both Pc ligands. Red cross in 1a indicate randomly distributed $Y[C_6S\text{-}Pc]_2$ molecules on Au surface.

Structures: Figure 1b shows the chemical structure of $Y[C_6S\text{-}Pc]_2$ where a Y^{3+} ion is sandwiched between two phthalocyanine (Pc) rings. Both Pc rings are fully peripherally substituted with S linked C_6H_{13} groups. They are oppositely domed and rotated by approximately 45° with respect to each other. The structure of $Y[C_4O\text{-}Pc]_2$ is similar with O replacing S. The optimized structure of $Y[HS\text{-}Pc]_2$ is shown in Figure 1 c and d. This simplified structure was used to probe the electronic and structural properties of the core complex.

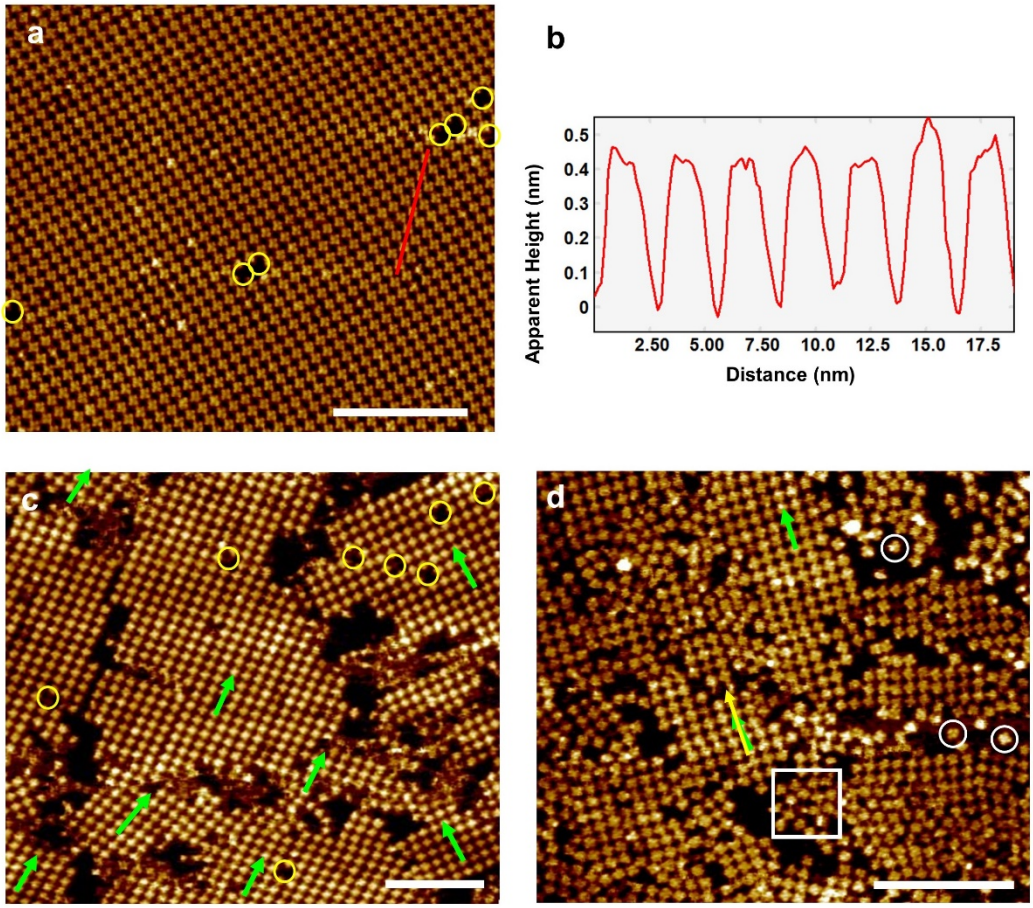

Figure 2: Surface-assisted self-assembly of $Y[C_6S\text{-}Pc]_2$ on top of HOPG and Au(111) surfaces at room temperature. a) Large scale STM images of $Y[C_6S\text{-}Pc]_2$ self-assembled architectures (a) at PO/HOPG interface and a cross section(b), indicated by red line in a. STM images of $Y[C_6S\text{-}Pc]_2$ at the PO/Au(111) (c & d) interfaces. Yellow circles show surface vacancy defects, the white circles identify individual $Y[C_6S\text{-}Pc]_2$ molecule, while the white square shows grains of closely packed but disordered molecules. The green arrows depicts direction of orientation of small grains of $Y[C_6S\text{-}Pc]_2$ complex on Au(111) surface. Concentration of $Y[C_6S\text{-}Pc]_2$ solution is 10 µM for both HOPG and Au(111) surfaces. Scale bar in all images is 20 nm. Tunneling parameters: (a) V_{bias} = -1 V, I_{tunnel} = 20 pA; (b) V_{bias} = -0.7 V, I_{tunnel} = 20 pA; (d) V_{bias} = -0.7 V, I_{tunnel} = 20 pA.

STM Data: Firstly, we investigated the self-assembly of Y[C_6S-Pc]$_2$ complex by applying 10 µL of a 10 µM solution of Y[C_6S-Pc]$_2$ in 1-PO on a freshly cleaved HOPG surface. The Y[C_6S-Pc]$_2$ complex formed a long range ordered, and uniform monolayer at the 1-PO/HOPG interface (Figure 2a). A cross-section profile over a few molecules (Figure 2b) reveals that the height of molecule was approximately 0.40 ± 0.02 nm which is close to earlier reported studies of DD complexes (Figure S1).[48] Also, we observed a few surface defects in the form of molecular vacancies in monolayers of the Y[C_6S-Pc]$_2$ complex. These defects appear as holes with apparent depths of approximately 0.40 ± 0.03 nm which we believe are due to loss of a single molecule from the continuous monolayer (Figure S1).[24] Figures 2c and 2d show the STM of Y[C6S-Pc]2 on Au(111).

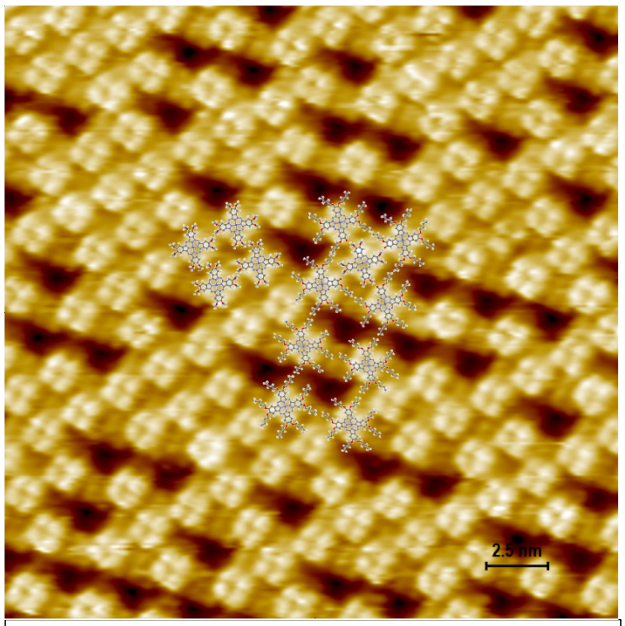

Figure 3: Y[C_4O-Pc]$_2$ monolayer at 30 µM in 1-PO and HOPG interface. Scaled molecules are inserted. Regions of open and dense square structures are typical. V_{bias} = 0.8 V, I= 20 pA

An STM image of a typical region of a monolayer of the interface between 30 µM Y[C_4O-Pc]$_2$ in 1-PO and HOPG is shown in Figure 3. This apparently disordered structure is composed of two well defined and interleaved structures present in different proportions across the surface. The long-range persistence of this structure can be seen most clearly in Figure S2. The surface is composed of an open 2.60±0.05 x 2.60±0.05 nm 90±2° structure that has molecules inserted in the opening in the center to produce a 1.86±0.05 x 1.86±0.05 90±2°. For this to occur the alkane chains of the O-C4 groups must extend up into solution rather than lie flat upon the surface as they do in the open structure. The phenomena of short ($\lesssim$ C12) alkane prosthetic groups failing to adsorb on HOPG is well documented.[49]

Remarkably, under similar concentration to those used for adsorption on HOPG, the Y[C_6S-Pc]$_2$ complex on Au(111) formed three types of molecular arrangements as shown in Figure 2b & 2d. Small ordered grains, disordered close-packed molecules (indicated by white square), and isolated single molecules (represented by white circles) were present on Au(111) surface. Single molecule vacancies (yellow circles) were also observed. The poorly ordered distribution of molecules on Au(111) suggests strong binding interaction between the Y[C_6S-Pc]$_2$ complex and Au(111) surface which results in rapid nucleation and growth of small ordered grains. The self-organized structures of Y[C_6S-Pc]$_2$ form a close packed square lattice structure on the HOPG surface. The lattice parameters were measured to be a = 2.1±0.05 nm, b = 2.1±0.05 nm, and angle = 92°±3°. The individual molecules seen in Figure 2d are not randomly oriented but instead are multiples of 15°

rotationally positioned. This can be seen more clearly in Figure S4. This 15 degree multiple interval is additional evidence of a preferred adsorption position of Y[C_6S-Pc]$_2$ on Au(111).

The cross-like molecule resembles a metallophthalocyanine with peripheral sulfurs, which is the top half of the Y[C_6S-Pc]$_2$ complex. High resolution STM images reveal flat adsorption of the DD complex on both HOPG and Au(111) surfaces, i.e., with the ligand planes parallel to the substrate surface (Figure 4), similar to monomeric alkylated phthalocyanines.[50] Four lobes forming cross shaped molecules were observed which corresponds to the four six-membered rings of the upper phthalocyanine unit in the Y[C_6S-Pc]$_2$ complex. In DD complexes, the lower Pc ligand is distant from the upper Pc ring, and even more distant from the tip, so it is not possible to tunnel directly into and clearly image the lower Pc ligand. Also, the substrate is even further away from the upper Pc ligand. Hence, the contribution of the substrate density of states, as well as that of the lower Pc ring, to the STM image is minimal, allowing easier observation of the orbital distribution in the upper Pc ligand.

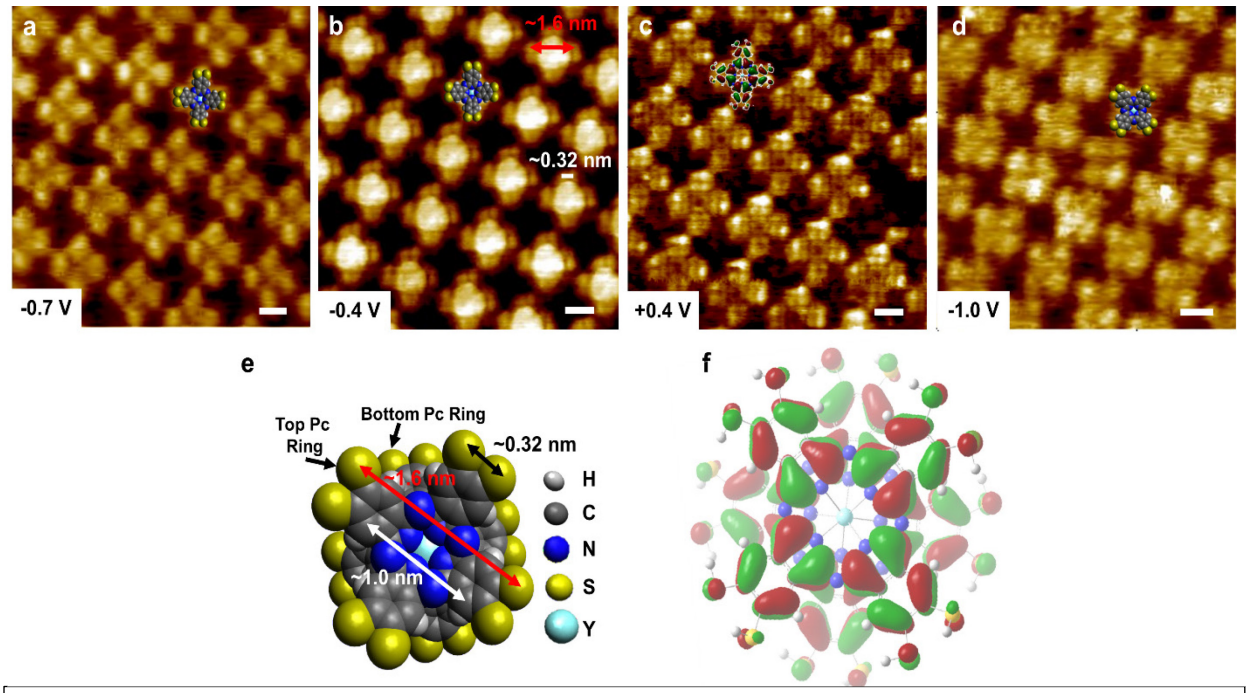

Figure 4: Submolecular resolution of Y[C_6S-Pc]$_2$ complex. High-resolution STM images revealing sub molecular features at 1-PO/HOPG (a, b, c), and 1-PO/Au(111) (d) interfaces at different bias voltage. Concentration of Y[C_6S-Pc]$_2$ solution is 10 µM for both HOPG and Au(111) surfaces. e) Structural model of Y[HS-Pc]$_2$ complex, where dark blue atoms are nitrogen, dark gray atoms are carbon, dark yellow atoms are sulfur, dark cyan atom is yttrium, and light gray atoms are hydrogen. f) The electron density distribution of the Y[HS-Pc]$_2$ LUMO calculated by density functional theory. For simplicity, here we have shown structure and LUMO level of Y[HS-Pc]$_2$ complex instead of Y[C_6S-Pc]$_2$. Also, schematic molecular structures of the corresponding top layers in the Y[C_6S-Pc]$_2$ complex without side chains were superimposed on STM images in a, b, and d. In STM image e, LUMO of top layer was superimposed. Scale bar is 1 nm in all STM images. Tunneling parameters: (a) V_{bias} = -0.7 V, I_{tunnel} = 10 pA; (b) V_{bias} = -0.4 V, I_{tunnel} = 20 pA; (c) V_{bias} = 0.4 V, I_{tunnel} = 20 pA (d) V_{bias} = -1 V, I_{tunnel} = 20 pA.

Figure 4c shows a real-space model of the Y[C_6S-Pc]$_2$ molecules where side chains of R= -C_6H_{13} are replaced with hydrogen atoms for simplicity of display and calculation. To gain more insight to intramolecular structure of our DD complex, high resolution STM images at different bias voltage and constant tunneling current at the 1-PO/HOPG interface are also displayed in Figure 4. Remarkably, at bias -0.4 V, the STM image shows eight lobes (Figure 4d). The distance between the two closest lobes is approximately 3.2 Å which agrees with the distance between two sulfur atoms present on one benzene ring of Y[C_6S-Pc]$_2$ calculated from the optimized DFT structure. Also, the distance between two diagonal lobes is ~1.6 nm which also matches to the DFT calculated value. At bias +0.4 V, STM images closely match the lowest unoccupied molecular orbital (LUMO) of the Y[C_6S-Pc]$_2$ complex (Figure 4f) which is due only to the upper Pc ligand. The HOMO and LUMO are quite similar (Figure S5) and one cannot dismiss the possibility that

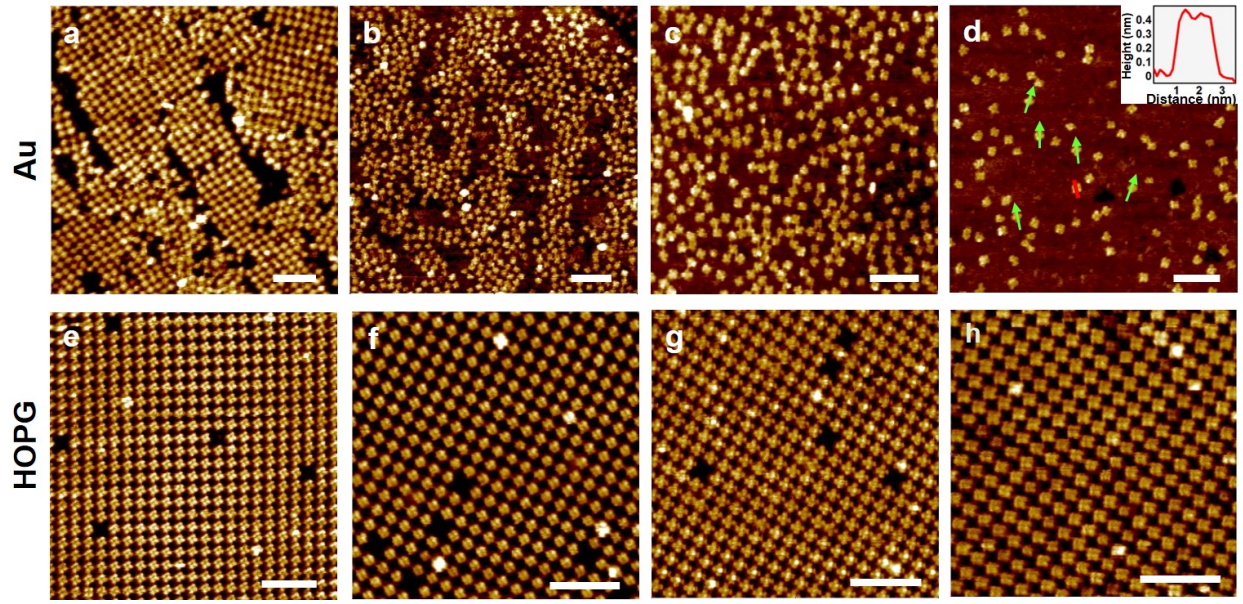

Figure 5: Concentration dependent self-assembly of Y[C_6S-Pc]$_2$ complex on Au(111) and HOPG surfaces. STM images of Y[C_6S-Pc]$_2$ complex at different concentrations: 10 µM (a), 5 µM (b), 1 µM (c), and 0.2 µM (d) at 1-PO/Au(111) interface. STM images of Y[C_6S-Pc]$_2$ complex at 1-PO/HOPG interface at different concentrations: 10 µM (e), 5 µM (f), 1µM (g), and 0.2 µM (h). Inset image in figure d shows the topographic STM height profile across individual Y[C_6S-Pc]$_2$ molecules (indicated by red line). Bright green arrows in STM image d indicates direction of orientation of individual molecule. Large areas of bare Au substrate were present at lower concentration. Scale bars in all images is 10 nm. Tunneling parameters: a) V_{bias} = -1.0 V, I_{tunnel} = 20 pA; (b-d) V_{bias} = -0.7 V, I_{tunnel} = 20 pA; (e) V_{bias} = -0.7 V, I_{tunnel} = 10 pA, (f) V_{bias} = -0.5 V, I_{tunnel} = 20 pA, (g) V_{bias} = -0.6 V, I_{tunnel} = 10 pA, (h) V_{bias} = -1.0 V, I_{tunnel} = 20 pA.

both contribute to the image at bias voltages near zero. The hydrocarbon portion of the side chains of Y[C_6S-Pc]$_2$ were not visible in STM images. A bit of a curiosity is the fact that the center of the molecule in Figure 4b is bright - unlike the dim center seen at the other voltages displayed. We suggest that this bright center might be due to resonant tunneling through mixed of yttrium metal and Pc valence orbitals, similar to what is seen in cobalt phthalocyanine.[30,51] If so, the

resonant tunneling it would result from changes in the yttrium electronic density of states because of interactions with the substrate and would not be observable in the gas phase calculation used to generate figure 4f.

The presence of small grains and isolated Y[C_6S-Pc]$_2$ molecules on the Au(111) surface but not on HOPG motivated us to investigate the effect of concentration on self-assembly. To determine that this presence was not a simple concentration effect, we performed STM imaging at different concentrations at both 1-PO/Au(111) and 1-PO/HOPG interfaces. Remarkably, we observed stable oriented and isolated Y[C_6S-Pc]$_2$ molecules with large empty space on the Au(111) surface at low concentration (0.2 μM) (Figure 5). The topographical height profile across an isolated molecule (the red lines in Figure 5d) shows an almost identical height of 0.4 nm compared to Y[C_6S-Pc]$_2$ molecules on the HOPG surface.[48] The same concentration on the HOPG surface produces a very different result. Here one finds large open areas with small regions of fully formed but unstable monolayer packing. The resulting distribution is quite like that of Y[C_4O-Pc]$_2$ on HOPG (Figure S3) and on Au (vide infra).

When intermolecular interactions are stronger than the molecule-substrate interaction, molecules diffuse about the surface until aggregation into islands immobilizes them. If the adsorbate-substrate interactions are sufficiently weak, few nucleation sites form and large well-ordered islands result. In these cases, thermodynamics can control the observed structure.[52] When the molecule-substrate interaction is very strong, the steady state coverage is achieved with randomly distributed isolated molecules because the barrier to diffusion across the surface is high compared to k. In these cases, the surface structure is controlled by kinetics and the thermodynamic equilibrium structure cannot be achieved. If one were to heat the kinetically controlled system sufficiently, one would expect it to convert to the thermodynamic equilibrium state. The observed structural disorder and presence of isolated molecules only in the sulfur linked system confirms that the Y[C_6S-Pc]$_2$-Au interactions are much stronger than the Y[C_6S-Pc]$_2$ -HOPG interactions and stronger than the Y[C_6S-Pc]$_2$ - Y[C_6S-Pc]$_2$ interactions.

S-linked versus O-linked: The above observation that Y[C_6S-Pc]$_2$ binds more strongly to Au than to HOPG leads one to ask if this strong affinity for Au(111) is a common phenomenon for all DD complexes, or is it specific to sulfur linked systems? To answer this question, we compared STM studies of a non-sulfur linked DD complex, Y[C_4O-Pc]$_2$, on the Au(111) surface (Figure 6). Figure 6a is a model of the compound, while Figures 6b-6f are STM images of Y[C_4O-Pc]$_2$, on the Au(111). At 1 μM concentration of Y[C_4O-Pc]$_2$ on Au(111), small islands are observed with the same 2.60±0.05 x 2.60±0.05 nm 90±2° structure seen on HOPG but these islands are not stable. Figure 6e and 6f show two consecutive scans of the same area. Molecules present in the blue dotted rectangle disappeared in the 2nd scan. Isolated molecules were not observed. This indicates much weaker interaction between Au(111) and Y[C_4O-Pc]$_2$ relative to the sulfur analog. This is in stark contrast to the behavior of the Y[C_6S-Pc]$_2$ complex. We again note that the distribution Y[C_4O-Pc]$_2$ complex on Au parallels nicely the behavior of Y[C_6S-Pc]$_2$ on HOPG. Thus, it appears that the high affinity of Y[C_6S-Pc]$_2$ for Au(111) is related to the sulfur linkers.

Having determined that the sulfur linkers are providing the strong attachment to the Au surface, one must ask what is the primary factor contributing to this affinity? While it is well known that thiols and disulfides form strong covalent bonds with a gold surface[53], the interaction of organic sulfides with gold is less well known. Two types of organic sulfides, thiophene and di-alkylsulfides, have been explored. In direct conflict with early theoretical predictions, Dishner et al. were able to observe STM images of self-assembly of thiophene on Au(111) by immersion in an ethanolic solution.[54] Following Dishner's work, several authors investigated the thiophene-Au(111) system and determined that at low coverages the molecule adsorbed reversibly (no S-C bond cleavage) and that the thiophene lay nearly parallel to the gold surface.[55-57] Temperature-programmed desorption measurements indicate that the reversible desorption energy is near 0.65 eV.[55,57] More recent density functional treatments of the thiophene-Au(111) system give reasonable agreement with experiment.[43,58] A small but informative body of literature also exists for the dialkylsufides adsorbed on gold. These studies also indicate that the dialkylsulfides adsorb reversibly without cleavage of the S-C bonds and that the alkane chains tend to lay parallel to the surface at low surface coverage.[41,59,60] Interestingly, diethylsulfide is reported to have a desorption energy larger than for thiophene.[61] While computational studies are hard to find, they do exist.[41]

While an adsorption energy of the order of 0.7 eV in UHV is unlikely to result in strong adsorption from solution, one must remember that each DD has eight sulfurs in contact with Au. An 8×0.7 eV adsorption energy is very strong. To put this in perspective, however, we should contrast this adsorption energy of thiophene and dimethylsulfide with that of similar oxygen compounds -- furan and dimethylether. To this end we have performed periodic boundary condition DFT calculations on thiophene, furan, dimethylsulfide and dimethylether adsorbed in a near planar configuration on unreconstructed Au(111) and on HOPG. Table 1 contains the results of these calculations and Figures S10, S11, and S12 show a selection of local minima and their associated desorption energies.

Based on the results reported in Table 1, the S linked system has an adsorption energy of 0.1 to 0.3 eV greater than the oxygen analog, per linker. Taking the lower value, 0.1 eV per S, gives an increased adsorption energy of 77 kJ/mol for the S linked DD over the O linked DD. We believe that it is this strong reversible interaction of the valence saturated sulfur that makes the S linked double decker particularly stable on the Au surface. Going further, we suggest that these sulfur linked systems may be generally useful for creating strong adsorption on gold without cleaving existing chemical bonds.

What about the difference between Au(111) and HOPG? To address this issue, we computed the adsorption energies of the same compounds on HOPG. The resulting values are given in Table 1. Elkington and Curthoys used gas chromatography to measure the heats of adsorption of both thiophene and furan on carbon black.[62] Assuming the absence of an activation barrier to adsorption, adsorption and desorption energies should be similar. Their results are also reported in Table 1. While the values are smaller than the calculated ones, both results for furan and thiophene are similar on a given surface. Shukla and coworkers measured the desorption energy

of diethyl ether on graphite by temperature programmed desorption. [63] Their result is included in Table 1. Son and Rybolt,[64]provided both computational and experimental values for the binding energy of thiophen on graphite. While the experimental data on heats of adsorption is incomplete, and our DFT calculations appear to overestimate the adsorption energies, it is clear that the covalently saturated sulfur species adsorb with similar energies on HOPG and with significantly higher energies on HOPG when compared to the covalently saturated oxygen analogs. These results are entirely consistent with our STM observations.

Table 1: Electronic desorption energies (eV) for the indicated molecules in a near planar configuration on Au(111) and on HOPG.

	Au(111)		HOPG	
Adsorbate	This work	Previous	This work	Previous
Thiophene	0.67	0.63[a]	0.57	0.35[c]
Furan	0.58	0.51[b]	0.51	0.31[d]
Dimethylsulfide	0.77	(0.70[f])	0.48	
Dimethylether	0.47		0.45	(0.47[e])

a) Experimental from reference 61; b) computational from reference43; c) experimental value from reference64; d) experimental from reference 62; e) experimental value for diethylether from reference 63, and f) experimental value for diethylsulfide from reference 61.

The strength of adsorption is suggestive, but not necessarily predictive, of low diffusion barriers on surfaces. To ensure that the S-Au interactions are inhibiting molecular translations on Au, we used DFT to estimate the barriers to translation for dimethylsulfide and dimethylether. This was done by starting from the optimized lowest energy bound structure and then simply translating the adsorbate to one of the symmetrical midpoints to the next equivalent position on the surface. There a single point energy calculation was performed. Some of the structures and results are presented in Figures S13, S14, and S15. Based on these calculations, the barrier to translation for dimethyl sulfide on Au(111) is 2.2 times higher (about 0.22 V) for the thiol than for the ether. Given that motion of the $Y[C_6S\text{-}Pc]_2$ required the translation of eight disulfides, it is clear that these calculations strongly support the near immobility of the $Y[C_6S\text{-}Pc]_2$ complex on Au. Interestingly, the barrier to translation for dimethylether on HOPG is only about 0.02 V (S14).

Surface and Tip-Induced Defects on HOPG: To determine the stability of the self-assembled structure on the HOPG surface, we investigated the effect of bias voltage, tunneling current, and time on the monolayer and surface vacancies. Consecutive STM scanning of the same area at different bias but at constant tunneling current, reveals a large change in number of surface vacancies Figure S6 and S7). Upon varying the bias from -1.0 V to -0.7 V at tunneling current = 20 pA, a large increase in the number of vacancies was observed. This increase is likely due to desorption of molecules from the monolayer. Most importantly, when bias was switched back to its initial value i.e. -1.0 V, the number of defects decreased but the position of the few remaining

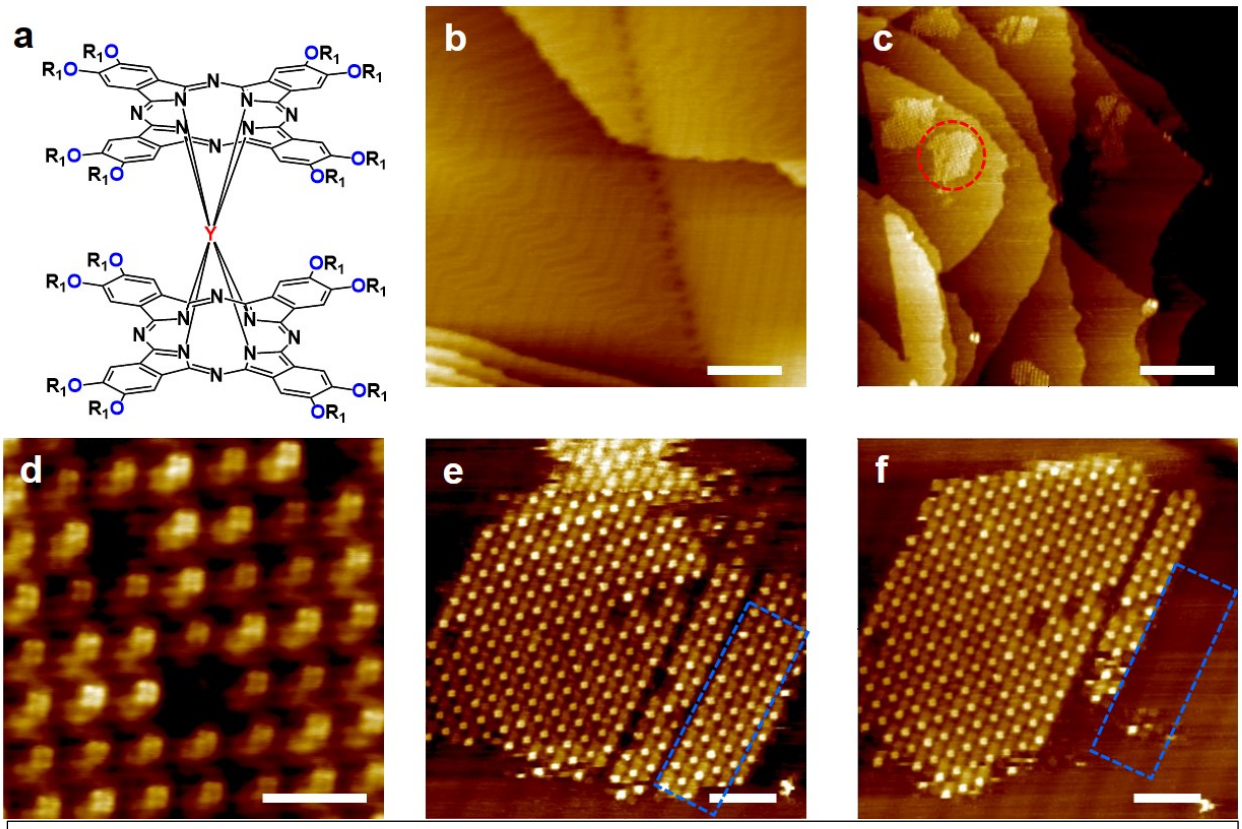

Figure 6: Surface-assisted self-assembly of Y[C_4O-Pc]$_2$ on top of Au(111) surfaces at room temperature. a) Molecular structure of Y[C_4O-Pc]$_2$, (b) resentative STM image of annealed Au(111) surfaces exhibit the well-known herringbone reconstruction lines. c) Large scale STM images of Y[C_4O-Pc]$_2$ complex architectures at 1-PO/Au(111). Red dotted circle indicates island of Y[C_4O-Pc]$_2$ complex on Au(111) surface. d) High resolution STM image of island of Y[C_4O-Pc]$_2$ on 1-PO/Au(111) interface. Dotted blue rectangle indicates group of molecules which are desorbed in consecutive scan. e and f) Consecutive STM images of islands of Y[C_4O-Pc]$_2$ on Au(111) surface reveals unstable nature of assembly. Here concentration of Y[C_4O-Pc]$_2$ solutions is 1 µM. Scale bar: b = 20 nm; c = 50 nm; d = 5 nm; e) & f) = 10 nm. Tunneling parameters: (a) V_{bias} = -1 V, (b) I_{tunnel} = 20 pA; (c) V_{bias} = -0.7 V, I_{tunnel} = 20 pA; (d) V_{bias} = -0.7 V, I_{tunnel} = 20 pA.

defects has changed (Figure 7). To check the reproducibility, the same procedure was again repeated between -1.0 V and -0.7 V, every time the same results were observed. Changing the bias polarity does not have a significant influence on stability of the monolayer, orientation, and number of surface defects (Figure S8). A monolayer was stable in bias ranging from -0.5 V to -1.0 V and from +0.5 V to +1.0 V (Figure S8). Similarly, to study the effect of tunneling current, sequential scans of the same area at constant bias but at different tunneling current ranging from 20 pA to 250 pA was performed. The monolayer was quite stable up to 100 pA, and also the number of vacancies was not greatly changed. Beyond 150 pA, desorption of the monolayer began but switching back to 20 pA caused redeposition and gives a well order structure with no change

in orientation (Figure S8). Overall, switching the scanning conditions to those normally used to see assembly caused redeposition of DD molecules on HOPG surface.

Increasing the tunneling current or decreasing the bias voltage causes the tip to move closer to the surface. This motion could result in physical contact between tip and molecules, producing a disturbance in the monolayer and causing desorption of molecules from the HOPG surface. Alternatively, the desorption could be the result of the electric field generated by the tip. In this case, the analysis is more complicated because increasing the voltage at fixed bias increases the distance, *d*, between tip and surface while the electric field goes as *V*/*d*. An even greater complicating factor is the fact that the current depends on the local density of states and that also changes with voltage. The logarithmic plots of the tunneling current versus *d* at fixed bias are not linear and have increasing slope as the tip-surface distance decreases. These non-linear plots suggest that understanding the voltage and current dependence of the tip induced desorption will require a detailed analysis of the LDOS of this system – an analysis we are not prepared to make at this time.

Given the empirical observation that vacancies depend upon bias conditions, one may ask about the time evolution of defect formation and repair. To gain insight into this process, we sequentially scanned the same area of the interface for several minutes at constant bias -0.7 V and a tunneling current 10 pA. The diffusion, disappearance, and generation of new vacancies was observed. Most vacancies remain at their initial position during sequential scanning (Figure 8a to 8j) while some vacancies (red arrows in Figure 8) moved. Initially, vacancy 7 & 8 in Figure 8 are separated by six molecules but in image 8c the distance is reduced to three because three DD molecules slide towards vacancy 8. Then in image 8e, vacancy 7 moved one placed towards right as indicated by yellow arrows. Some molecules appeared to be blinking, i.e., desorption and adsorption behavior of molecules from solution. A molecule indicated by a green circle in Figure 8g disappeared but reappeared in Figure 8j. Initially, the total number of vacancies are eight but in the final image there are nine i.e. one new vacancy is formed. It is indicated by a white circle (Figure 8g). Thus, each consecutive scan at -0.7 V bias will not generate new vacancies in every scan. Here observed diffusion of vacancies is mostly due to sliding of molecules present next to a vacancy. These surface diffusion events are mostly occurring in the fast scan direction, indicating tip induced movement of molecules. Therefore, most of the observed vacancy mobility is a simple diffusion process, not an adsorption/desorption phenomenon.

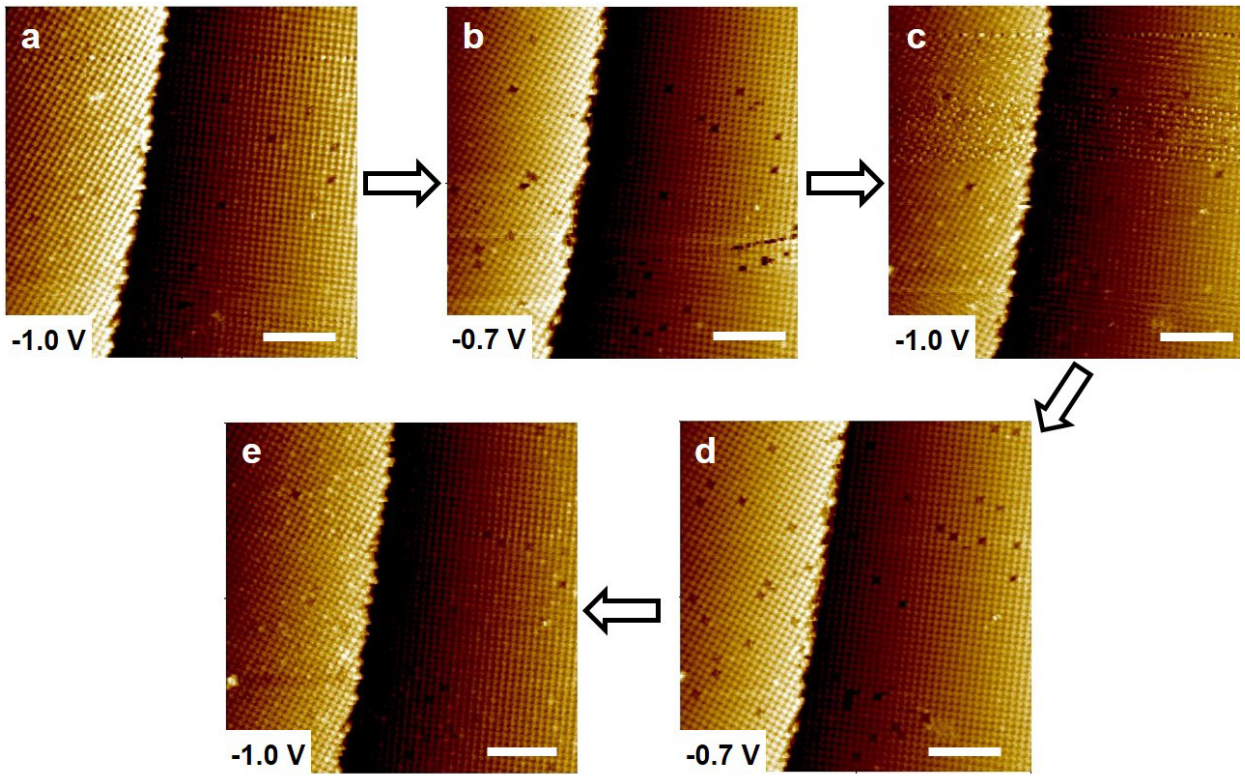

Figure 7: Effect of bias voltage on surface vacancy defects. Sequential STM images obtained at the same area of monolayer of $Y[C_6S\text{-}Pc]_2$ complex on the 1-PO/HOPG interface at different bias voltage and constant tunneling current (20 pA). Initially, bias voltage is -1.0 V and 20 pA tunneling current. Then bias is changed to -0.7 V but tunneling current is kept constant. The change of tip bias immediately induced a desorption of few molecules from HOPG surface and generated few more vacancy in the monolayer. Bias was again changed to -1.0 V without disturbing the tunneling current. The number of vacancies in the monolayer was reduced. The time interval among each image is 85 sec. The concentration of $Y[C_6S\text{-}Pc]_2$ solutions is 10 µM. Scale bar in all images is 20 nm.

In order to assess the role of thermally induced diffusive, we did a single STM image of a fixed area and then did not scan until 20 minutes later (Figure S9). Our hypothesis is that during that 20 minutes all motion would be due to thermal events since the tip was not perturbing the surface. Fascinatingly, about half the vacancies remained in their original positions, but some changed their position and a few new vacancies also appeared. Thus, a significant fraction of the vacancy motion is thermally induced. Extracting the kinetics of the thermally induced processes will be an extremely challenging problem since the time scales of the tip induced and thermal processes are very similar. The act of measuring the system disturbs.

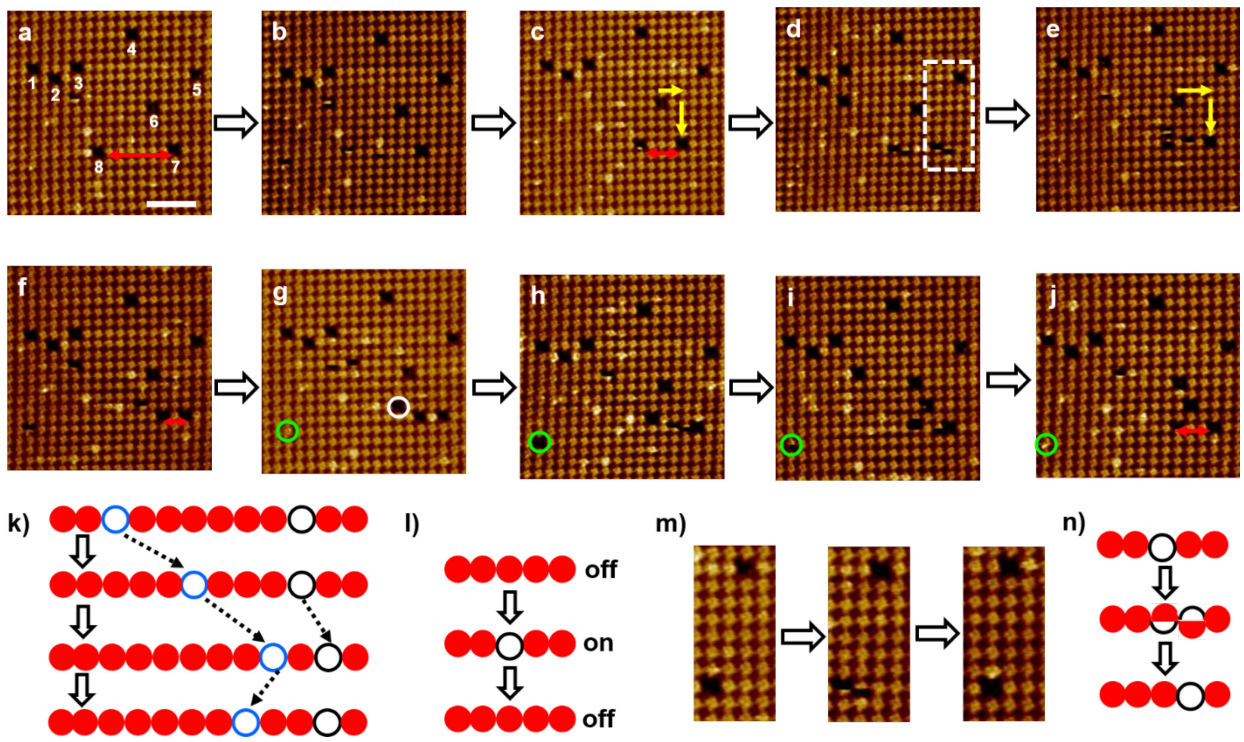

Figure 8: Effect of scanning on surface vacancy. Consecutive STM images of same area of a monolayer of Y[C_6S-Pc]$_2$ complex on 1-PO/HOPG interface at constant bias (-0.7 V) and tunneling current (10 pA) (a-j). Six vacancies (1 to 6) remained in their same position that they occupied in 1st scan. (k) shows schematic representations of the single and triple vacancy jump processes. (l) shows schematic description of desorption (on) and adsorption (off) of molecules from solution which is indicated by green circle. (m) represents zoomed-in portion of area represented by white dotted rectangle from image (c), (d), and (e) where sliding of molecule was clearly observed in middle image. (n) shows schematic illustrations of sliding of molecules. Red double headed arrow shows separation between vacancy 7 and 8, which is initially separated by six molecules than reduced to three, one and finally two. Yellow arrows show movement of vacancy 7. White circle represents a new vacancy. The time interval between the two images is 64 sec. The concentration of Y[C_6S-Pc]$_2$ solutions is 10 µM. Scale bar in all images is 10 nm. Tunneling parameters for all images are V_{bias} = -0.7 V, I_{tunnel} = 10 pA, and scan speed = 8 lines/sec.

4. CONCLUSIONS

The spontaneous adsorption of Y[C_6S-Pc]$_2$ and Y[C_4O-Pc]$_2$ on HOPG and Au(111) surfaces has been characterized by STM at solution-solid interface. Clear resolution of the internal structures of individual molecules was achieved. This is the highest resolution of a double-decker complex seen at the solution/solid interface to date. On HOPG well-ordered monolayers of Y[C_6S-Pc]$_2$ are observed at concentrations of 10 µM or more. At lower concentrations well-ordered but somewhat unstable islands are observed. This is also the case for Y[C_4O-Pc]$_2$ on HOPG and Au(111). Thus, intermolecular forces play a dominant role in the adsorption of Y[C_4O-Pc]$_2$ on either substrate. However, Y[C_6S-Pc]$_2$ on Au(111) nucleates much more rapidly and its mobility is dramatically

reduced. This is seen in the form of many small islands oriented relative to each other at multiples of 15 degrees at high concentration and by stable isolated molecules at very low concentration. Thus adsorption of Y[C_6S-Pc]$_2$ on Au(111) is dominated by molecular-substrate forces. Both the adsorption energy and the barrier to diffusion on Au(111) are substantially higher than for the oxygen linked compound. Thus, the structure of the sulfur linked complex on gold is kinetically controlled while all the other structures are likely thermodynamically stable. The strong Y[C_6S-Pc]$_2$-Au interaction is attributed to the sulfur linkers and not to the double deckers themselves. DFT calculations show that valence saturated sulfur compounds have significantly higher adsorption energies on gold than their oxygen analogs. The influence of the linking atoms may be significantly further enhanced by the lack of planarity of the distorted phthalocyanine ring which reduced the van der Walls interactions between the ring and the surface. It is suggested that core moieties having S-linked peripheral groups will generally be more strongly adsorbed on gold than with the same core compounds having oxygen linked peripheral groups. The marked difference in chemistry of the sulfide and oxide species on Au can play an important role in designing self-assembling surface structures where a particular core entity is chosen for its electronic or magnetic properties but requires prosthetic groups to self-assemble.

The monolayer of Y[C_6S-Pc]$_2$ on HOPG contains surface vacancy defects which are partially controlled by bias voltage and tunneling current and are partially thermally induced. We expect our report to encourage further research in the area of surface assemblies and the construction of molecular electronic devices.

AUTHOR INFORMATION

Corresponding Author

K W Hipps - Department of Chemistry and Materials Science and Engineering Program, Washington State University, Pullman, WA 99163-4630. orcid.org/ 0000-0002-5944-5114; Email: hipps@wsu.edu.

Authors

Shammi Rana - Department of Chemistry, Washington State University, Pullman, WA 99163-4630.

Jianzhuang Jiang - Department of Chemistry, University of Science and Technology Beijing, Beijing, 100083, China. jianzhuang@ustb.edu.cn.

Katalin V. Korpany - Department of Chemistry, Washington State University, Pullman, WA 99163-4630. katalin.korpany@wsu.edu. orcid.org/0000-0002-9058-8500

Ursula Mazur - Department of Chemistry and Materials Science and Engineering Program, Washington State University, Pullman, WA 99163-4630. Orcid.org/ 0000-0002-3471-4883

SUPPORTING INFORMATION

The Supporting Information is available free of charge at XXXXX. It contains details on the measurement of molecular height, pictures of HOMO and LUMO, and examples of bias voltage and set point current on the formation of defects. Also shown is a high-resolution image of isolated $Y[C_6S\text{-}Pc]_2$ molecules on Au indicating their 15° orientation relationship. Supercells of fully optimized adsorbates on Au(111) and their associated desorption energies are shown. Selected structures and their energies used to estimate the surface diffusion barrier are also given.

ACKNOWLEDGMENTS

We gratefully acknowledge support for this research from the US National Science Foundation in the form of grant CHE-1807225. We also gratefully acknowledge support from the W. M. Keck Foundation.

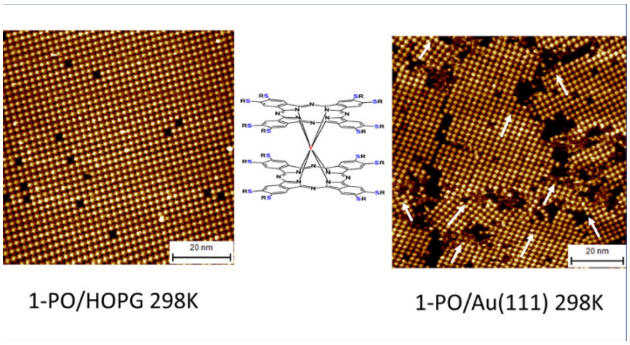

TOC Graphic

REFERENCES

(1) Kudernac, T.; Lei, S. B.; Elemans, J.; De Feyter, S. Two-Dimensional Supramolecular Self-Assembly: Nanoporous Networks on Surfaces. *Chem. Soc. Rev.* **2009,** *38*, 402–421.

(2) De Feyter, S.; De Schryver, F. C. Self-Assembly at the Liquid/Solid Interface: STM Reveals. *J. Phys. Chem. B* **2005,** *109*, 4290–4302

(3) Lewis, P. A.; Donhauser, Z. J.; Mantooth, B. A.; Smith, R. K.; Bumm, L. A.; Kelly, K. F.; Weiss, P. S. Control and Placement of Molecules via Self-Assembly. *Nanotechnology* **2001**, *12*, 231–237.

(4) Ferreira, Q.; Delfino, C. L.; Morgado, J.; Alcácer, L. Bottom-Up Self-Assembled Supramolecular Structures Built by STM at the Solid/Liquid Interface. *Materials* **2019***, 12*, 382–403.

(5) Auwärter, W.; Écija, D.; Klappenberger, F.; Barth, J. V. Porphyrins at Interfaces. *Nat. Chem.* **2015,** *7*, 105−120.

(6) Ciesielski, A.; Szabelski, P. J.; Rzysko, W.; Cadeddu, A.; Cook, T. R.; Stang, P. J.; Samorì, P. Concentration-Dependent Supramolecular Engineering of Hydrogen-Bonded Nanostructures at Surfaces: Predicting Self-Assembly in 2D. *J. Am. Chem. Soc.* **2013,** *135*, 6942−6950.

(7) Doudevski, I.; Schwartz, D. K. Concentration Dependence of Self-Assembled Monolayer Island Nucleation and Growth. *J. Am. Chem. Soc.* **2001,** *123*, 6867−6872.

(8) Hu, F.; Gong, Y.; Zhang, X.; Xue, J.; Liu, B.; Lu, T.; Deng, K.; Duan, W.; Zeng, Q.; Wang, C. Temperature-Induced Transitions of Self-Assembled Phthalocyanine Molecular Nanoarrays at the Solid–Liquid Interface: From Randomness to Order. *Nanoscale* **2014,** *6*, 4243–4249.

(9) Jingfei, H.; Peng, L.; Ting, M.; Fengying, Z.; Haijun, X.; Xiaokang, L.; Ke, D.; Qingdao, Z. Solvent-Dependent Self-Assemblies and Pyridine Modulation of a Porphyrin Molecule at Liquid/Solid Interfaces. *Langmuir* **2020,** *36*, 9810−9817.

(10) Chen, C.; Zhang, S.; Tu, B.; Meng, T.; Li, J.; Qian, Y.; Li, P.; Liu, B.; Duan, W.; Xu, H.; et al. Solvent Dependent Core-Modified Rubyrin Self-Assembly at Liquid/Solid Interfaces. *Langmuir* **2020,** *36*, 3879−3886.

(11) Kühnle, A. Self-Assembly of Organic Molecules at Metal Surfaces. *Curr. Opin. Colloid Interface Sci.* **2009,** *14*, 157−168.

(12) Liu, C. H.; Yang, L.; Wang, Y.; Lei, S. B.; Hu, W. P. Substrate Effects in the Supramolecular Self-Assembly of 2,4,6-Tris(4-bromophenyl)-1,3,5-triazine on Graphite and Graphene. *J. Phys. Chem. C* **2018,** *122*, 12307−12314.

(13) Balandina, T.; Tahara, K.; Sandig, N.; Blunt, M. O.; Adisoejoso, J.; Lei, S. B.; Zerbetto, F.; Tobe, Y.; De Feyter, S. Role of Substrate in Directing the Self-Assembly of Multicomponent Supramolecular Networks at the Liquid-Solid Interface. *ACS Nano* **2012,** *6*, 8381−8389.

(14) Komeda, T.; Katoh, K.; Yamashita, M. Double-Decker Phthalocyanine Complex: Scanning Tunneling Microscopy Study of Film Formation and Spin Properties. *Prog. Surf. Sci.* **2014,** *89*, 127−160.

(15) Gottfried, J. M. Surface Chemistry of Porphyrins and Phthalocyanines. *Surf. Sci. Rep.* **2015,** *70*, 259−379.

(16) Qian, Y.; Liu, B.; Duan, W.; Zeng, Q. Assemblies of Porphyrin and Phthalocyanine Derivatives Studied by STM. *J. Porphyrins Phthalocyanines* **2018,** *22*, 717–725.

(17) Jiang, J.; Ng, D. K. P. A Decade Journey in the Chemistry of Sandwich-type Tetrapyrrolato-Rare Earth Complexes. *Acc. Chem. Res.* **2009,** *42*, 79−88.

(18) Ishikawa, N.; Sugita, M.; Ishikawa, T.; Koshihara, S.; Kaizu, Y. Lanthanide Double-Decker Complexes Functioning as Magnets at the Single-Molecular Level. *J. Am. Chem. Soc.* **2003,** *125*, 8694–8695.

(19) Gonidec, M.; Biagi, R.; Corradini, V.; Moro, F.; De Renzi, V.; del Pennino, U.; Summa, D.; Muccioli, L.; Zannoni, C.; Amabilino, D.; et al. Surface Supramolecular Organization of a Terbium(III) Double-Decker Complex on Graphite and its Single Molecule Magnet Behavior. *J. Am. Chem. Soc.* **2011,** *133*, 6603–6612.

(20) Schwöbel, J.; Fu, Y.; Brede, J.; Dilullo, A.; Hoffmann, G.; Klyatskaya, S.; Ruben, M.; Wiesendanger, R. Real-Space Observation of Spin-Split Molecular Orbitals of Adsorbed Single-Molecule Magnets. *Nat. Commun.* **2012,** *3*, 953–957.

(21) Komeda, T.; Isshiki, H.; Liu, J.; Katoh, K.; Yamashita, M. Variation of Kondo Temperature Induced by Molecule−Substrate Decoupling in Film Formation of Bis(phthalocyaninato)terbium(III) Molecules on Au(111). *ACS Nano* **2014,** *8*, 4866−4875.

(22) Mannini, M.; Bertani, F.; Tudisco, C.; Malavolti, L.; Poggini, L.; Misztal, K.; Menozzi, D.; Motta, A.; Otero, E.; Ohresser, P.; et al. Magnetic Behaviour of $TbPc_2$ Single-Molecule Magnets Chemically Grafted on Silicon Surface. *Nat. Commun.* **2014,** *5*, 4582−4589.

(23) Vitali, L.; Fabris, S.; Mosca Conte, A.; Brink, S.; Ruben, M.; Baroni, S.; Kern, K. Electronic Structure of Surface-supported Bis(phthalocyaninato) Terbium(III) Single Molecular Magnets. *Nano Lett.* **2008,** *8*, 3364−3368.

(24) Miyake, K.; Fukuta, M.; Asakawa, M.; Hori, Y.; Ikeda, T.; Shimizu, T. Molecular Motion of Surface-Immobilized Double-Decker Phthalocyanine Complexes. *J. Am. Chem. Soc.* **2009,** *131*, 17808−17813.

(25) Otsuki, J.; Komatsu, Y.; Kobayashi, D.; Asakawa, M.; Miyake, K. Rotational Libration of a Double-Decker Porphyrin Visualized. *J. Am. Chem. Soc.* **2010,** *132*, 6870−6871.

(26) Zhang, Y.; Kersell, H.; Stefak, R.; Echeverria, J.; Iancu, V.; Perera, U. G. E.; Li, Y.; Deshpande, A.; Braun, K.-F.; Joachim, C.; et al. Simultaneous and Coordinated Rotational Switching of all Molecular Rotors in a Network. *Nat. Nano.* **2016,** *11*, 706−713.

(27) Otsuki, J. STM Studies on Double and Triple-decker Porphyrin and Phthalocyanine Complexes. *Supramol. Chem.* **2011,** *23*, 169−182.

(28) Takami, T.; Ye, T.; Pathem, B. K.; Arnold, D. P.; Sugiura, K.; Bian, Y. Z.; Jiang, J. Z.; Weiss, P. S. Manipulating Double-Decker Molecules at the Liquid-Solid Interface. *J. Am. Chem. Soc.* **2010,** *132*, 16460 −16466.

(29) Ma, H.; Ou Yang, L.-Y.; Pan, N.; Yau, S.-L.; Jiang, J.; Itaya, K. Ordered Molecular Assemblies of Substituted Bis-(phthalocyaninato) Rare Earth Complexes on Au(111): In Situ Scanning Tunneling Microscopy and Electrochemical Studies. *Langmuir* **2006,** *22*, 2105–2111.

(30) Lu, X.; Hipps, K. W. Scanning Tunneling Microscopy of Metal Phthalocyanines: d^6 and d^8 Cases. *J. Phys. Chem. B* **1997,** *101*, 5391–5396.

(31) Barlow, D.; Hipps, K. W. Orbital Mediated Tunneling in Vanadyl Phthalocyanine Observed in Both Tunnel Diode and STM Environments. *J. Phys. Chem. B* **2000**, *104*, 2444–2447.

(32) Huang, C.; Zhang, Y.; Sun, J.; Bian, Y.; Arnold, D. Bis/tris[octakis(hexylthio)phthalocyaninato] Europium(III) Complexes: Structure, Spectroscopic, and Electrochemical Properties. *J. Porphyrins Phthalocyanines* **2013**, *17*, 673–681.

(33) Wang, K.; Qi, D.; Wang, H.; Cao, W.; Li, W.; Liu, T.; Duan, C.; Jiang, J. Binuclear Phthalocyanine-Based Sandwich-Type Rare Earth Complexes: Unprecedented Two π-Bridged Biradical-Metal Integrated SMM. *Chem. - Eur. J.* **2013**, *19*, 11162–1166.

(34) Kresse, G.; Furthmüller, J. Efficiency of Ab-Initio Total Energy Calculations for Metals and Semiconductors Using a Plane-Wave Basis Set. *Comput. Mater. Sci.* **1996**, *6*, 15–50.

(35) Kresse, D.; Joubert, D. From Ultrasoft Pseudopotentials to the Projector Augmented-Wave Method, *Phys. Rev. B: Condens. Matter Mater. Phys.* **1999**, *59*, 1758–1775.

(36) Frisch, M. J.; Trucks, G. W.; Schlegel, H. B.; Scuseria, G. E.; Robb, M. A.; Cheeseman, J. R.; Scalmani, G.; Barone, V.; Mennucci, B.; Petersson, G. A., et al. *Gaussian 09*, Revision D.01, Gaussian, Inc.: Wallingford CT, 2013.

(37) Blöchl, P. E. Projector Augmented-Wave Method. *Phys. Rev. B* **1994**, *50*, 17953–17979.

(38) Klime, J.; Bowler, D. R.; Michaelides, A. Van der Waals Density Functionals Applied to Solids
Phys. Rev. B: Condens. Matter Mater. Phys. **2011**, *83*, 195131.

(39) Becke, A, D. Density-Functional Exchange-Energy Approximation with Correct Asymptotic Behavior. *Phys. Rev. A* **1988**, *38*, 3098–3100.

(40) Perdew, J. P.; Burke, K.; Ernzerhof, M. Generalized Gradient Approximation Made Simple. *Phys. Rev. Lett.* **1996**, *77*, 3865–3868.

(41) Tierney, H.; Calderon, C.; Baber, A. E.; Sykes, E.; Wan, F. Understanding the Rotational Mechanism of a Single Molecule: STM and DFT Investigations of Dimethyl Sulfide Molecular Rotors on Au(111). *J. Phys. Chem. C* **2010**, *114*, 3152–3155.

(42) Jahanbekam, A.; Chilukuri, B.; Mazur, U.; Hipps, K. W. A Kinetically Trapped Two-Component Self Assembled Adlayer. *J. Phys. Chem. C* **2015**, *119*, 25364–25376.

(43) Christian, M. S.; Otero-de-la-Roza, A.; Johnson, E. Surface Adsorption from the Exchange-Hole Dipole Moment Dispersion Model. *J. Chem. Theory Comput.* **2016,** *12*, 3305−3315.

(44) Chilukuri, B.; Mazur, U.; Hipps, K. W. Effect of Dispersion on Surface Interactions of Cobalt(II) Octaethylporphyrin Monolayer on Au(111) and HOPG(0001) Substrates: A Comparative First Principles Study. *Phys. Chem. Chem. Phys.* **2014**, *16*, 14096–14107.

(45) Borders, B.; Adinehnia, M.; Chilukuri, B.; Ruf, M.; Hipps, K. W.; Mazur, U.; Tuning Optoelectronic Characteristics of Ionic Porphyrin Crystalline Assemblies. *J. Mater. Chem. C* **2018**, *6*, 4041–4056.

(46) Adinehnia, M.; Borders, B.; Ruf, M.; Chilukuri, B.; Hipps, K.W.; Mazur, U. Comprehensive Structure-Function Correlation of Photoactive Ionic π-Conjugated Supermolecular Assemblies: An Experimental and Computational Study. *J. Mater. Chem. C* **2016**, *4*, 10223–10239.

(47) Zhang, Y. C.; Chilukuri, B.; Hanson, T.; Heiden, Z. B.; Lee, D. Y. Connecting Solution-Phase to Single-Molecule Properties of Ni(Salophen). *J. Phys. Chem. Lett.* **2019**, *10*, 3525–3530.

(48) Serrano, G.; Wiespointner-Baumgarthuber, S.; Tebi, S.; Klyatskaya, S.; Ruben, M.; Koch, R.; Mullegger, S. Bilayer of Terbium Double-Decker Single-Molecule Magnets. *J. Phys. Chem. C* **2016,** *120*, 13581−13586.

(49) Unlu, I.; Dixon, A. D.; Brozik, J. A.; Hipps, K. W. Alkynyl Linkers as a Design Tool to Gain Control Over Self-Assembly of Meso-Substituted Porphyrins on HOPG. *Langmuir* **2020**, *36*, 4897−4907.

(50) Qiu, X.; Wang, C.; Zeng, Q.; Xu, B.; Yin, S.; Wang, H.; Xu, S.; Bai, C. Alkane-Assisted Adsorption and Assembly of Phthalocyanines and Porphyrins. *J. Am. Chem. Soc.* **2000,** *122*, 5550−5556.

(51) Hipps, K. W. In *Handbook of Applied Solid State Spectroscopy*, Vij, D. R., Ed.; Springer Verlag **2006**, Chapter 7, pp. 305-350.

(52) Hipps, K. W.; Mazur, U. Kinetic and Thermodynamic Control in Porphyrin and Phthalocyanine Self-Assembled Monolayers. *Langmuir* **2018**, *34*, 3–17.

(53) Ulman, A. *An Introduction to Ultrathin Organic Films from Langmuir-Blodgett to Self-Assembly*; Academic Press: Boston, 1991.

(54) Dishner, M.; Hemminger, J.; Feher, F. J. Formation of a Self-Assembled Monolayer by Adsorption of Thiophene on Au(111) and Its Photooxidation. *Langmuir* **1996**, *12*, 6176–6178.

(55) Liu, G.; Rodriguez, J.; Dvorak, J.; Hrbek, J.; Jirsak, T. Chemistry of Sulfur-Containing Molecules on Au(111): Thiophene, Sulfur Dioxide, and Methanethiol Adsorption. *Surf. Sci.* **2002**, *505*, 295–307.

(56) Noh, J.; Ito, E.; Araki, T.; Hara, M. Adsorption of Thiophene and 2,5-Dimethylthiophene on Au(111) from Ethanol Solutions. *Surf. Sci.* **2003**, *532–535*, 1116–1120.

(57) Nambu, A.; Kondoh, H.; Nakai, I.; Amemiya, K.; Ohta, T. Film Growth and X-ray Induced Chemical Reactions of Thiophene Adsorbed on Au(111). *Surf. Sci.* **2003**, *530*, 101–110.

(58) Adhikari, S.; Tang, H.; Neupane, B.; Ruzsinszky, A.; Csonka, G. Molecule-Surface Interaction from van der Waals-Corrected Semilocal Density Functionals: The Example of Thiophene on Transition-Metal Surfaces. *Phys. Rev. Mat.* **2020**, *4*, 025005.

(59) Bellisario, D.; Jewell, A.; Tierney, H.E.; Baber, A.; Sykes, E. C. Adsorption, Assembly, and Dynamics of Dibutyl Sulfide on Au(111). *J. Phys. Chem. C* **2010**, *114*, 14583–14589.

(60) Noh, J.; Kato, H.; Kawai, M.; Hara, M. Surface and Adsorption Structures of Dialkyl Sulfide Self-Assembled Monolayers on Au(111). *J. Phys. Chem. B* **2002**, *106,* 13268–13272.

(61) Lavrich, D.J.; Wetterer, S.; Bernasek, S. L.; Scoles, G. Physisorption and Chemisorption of Alkanethiols and Alkyl Sulfides on Au(111). *J. Phys. Chem. B* **1998**, *102*, 3456–3465.

(62) Elkington, P.A.; Curthoys, G. Heats of Adsorption on Carbon Black Surfaces**.** *J. Phys. Chem.* 1**969** *73*, 2321–2325.

(63) Shukla, N.; Gui, J.; Gellman, A. Adsorption of Fluorinated Ethers and Alcohols on Graphite. *Langmuir* **2001**, *17*, 2395–2401.

(64) Son, H.; Rybolt, T. R. Force Field Based MM2 Molecule-Surface Binding Energies for Graphite and Graphene. *Graphene*, **2013**, *2*, 18–34.